Annual Methodological Archive Research Review
http://amresearchreview.com/index.php/Journal/about
Volume 4, Issue 6 (2026)

Online ISSN 3007-3197
Print ISSN 3007-3189

http://amresearchreview.com/index.php/Journal/about

GENOME-WIDE IDENTIFICATION AND CALCIUM STRESS-RESPONSIVE EXPRESSION OF TAOSCA GENES IN *TRITICUM AESTIVUM* VIA HYDROPONIC SYSTEM, WITH LOCALISATION OF TAOSCA.5 AND TAOSCA.10

Ali Murtaza*

Department of Plant Breeding and Genetics, University of Agriculture, Faisalabad, Pakistan.Corresponding Author Email: mralimurtazarai@gmail.com

Muhammad Tahsin

National Institute of Genomics and Advanced Biotechnology, NARC, Islamabad, Pakistan

Ayaz Haider Khan

Department of Plant Breeding and Genetics, University of Agriculture, Faisalabad, Pakistan

Maryam Alim

Institute of Horticultural Sciences, University of Agriculture, Faisalabad, Pakistan

Junaid Ahmad

Department of Plant Breeding and Genetics, University of Agriculture, Faisalabad, Pakistan

Rozia Gul

Department of Plant Breeding and Genetics, University of Agriculture, Faisalabad, Pakistan

ABSTRACT

Calcium (Ca^{2+}) is both an essential structural macronutrient and a universal intracellular second messenger in plants. The OSCA (Osmosensitive Calcium-Permeable Channel) gene family encodes putative mechanosensitive Ca^{2+} -permeable channels implicated in osmotic and ionic stress signalling; their expression under direct calcium stress in wheat has not been previously characterised by controlled experiment. Here we identify ten OSCA homologues (TaOSCA1–TaOSCA10) in *Triticum aesitivum L.* cv. Fakhr-e-Sarhad via BLAST

Annual Methodological Archive Research Review
http://amresearchreview.com/index.php/Journal/about
Volume 4, Issue 6 (2026)

Online ISSN 3007-3197
Print ISSN 3007-3189

http://amresearchreview.com/index.php/Journal/about

screening of the IWGSC-URGI database, and report expression profiling of the seven genes for which reliable qRT-PCR assays were established (TaOSCA.1, .2, .4, .5, .7, .9, .10). Phylogenetic analysis using the LG+G model across 227 OSCA sequences from Poaceae, Brassicaceae, and Malvaceae resolved three conserved sub-functional clades. Thirty-six plants were grown hydroponically (Lombnaes medium; pH 6.0–6.2; 22° C) under calcium deficiency (0 mM), optimal control (2 mM), and toxicity (8 mM) with harvests at D0, D7, D14, and D21. Both stress conditions significantly reduced whole-plant biomass (42% and 69% reduction at D21 for deficiency and toxicity respectively; $p < 0.01$), with characteristic chlorosis and stunted root development. Reference gene stability was validated by NormFinder before Pfaffl-method qRT-PCR analysis. Seven TaOSCAs were significantly differentially expressed (FDR $q < 0.05$). An osmotic specificity control at D7 (18 mM mannitol and 9 mM NaCl, matched to the osmolality and ionic strength of 8 mM $CaCl_2$ respectively) confirmed that expression changes are Ca^{2+} -specific rather than general osmotic or ionic-strength artefacts. Subcellular GFP-fusion localisation in Nicotiana benthamiana demonstrated exclusive plasma membrane localisation for TaOSCA.5 (Pearson's $r = 0.891$ with AtPIP2;1) and dual plasma membrane plus tonoplast distribution for TaOSCA.10 ($r = 0.714$ and 0.823 with AtPIP2;1 and AtVAM3, respectively).

Keywords: *Triticum aestivum*; TaOSCA; calcium stress; expression profiling; hydroponic system; qRT-PCR; LG+G phylogeny; subcellular localisation; osmotic control; NormFinder; MIQE; abiotic stress

Introduction

Wheat (*Triticum aestivum L.*) is the world's most widely cultivated cereal, providing approximately 20% of total human caloric intake and representing Pakistan's most critical staple crop, with production reaching 28.18 million tonnes in 2022–23 (Filip et al., 2023; Wakwaya & Alemu, 2023). Sustained yield improvements are constrained by abiotic stresses, including nutrient imbalances on Pakistan's predominantly calcareous soils where calcium (Ca^{2+}) availability varies from deficit to excess depending on irrigation source and soil pH (Murtaza et al., 2023; Rahim et al., 2024).

Annual Methodological Archive Research Review
http://amresearchreview.com/index.php/Journal/about
Volume 4, Issue 6 (2026)

Online ISSN 3007-3197
Print ISSN 3007-3189

http://amresearchreview.com/index.php/Journal/about

Ca^{2+} serves a uniquely dual function: as a structural macronutrient cross-linking pectin in cell walls and stabilising membranes,[4,5] and as a ubiquitous intracellular second messenger activating CDPKs, CaMs, and CBL–CIPK cascades that co-ordinate stress gene expression (Mirza, 2012). At optimal concentrations (typically 1–2 mM in nutrient solution), Ca^{2+} supports normal growth; deficiency produces chlorosis, necrotic leaf margins, and stunted roots, while excess Ca^{2+} competitively inhibits Mg^{2+} and K^{+} uptake and disrupts membrane integrity (Ahmed et al., 2023; Singh et al., 2017).

The OSCA gene family encodes putative mechanosensitive Ca^{2+} -permeable channels first characterised in *Arabidopsis thaliana* as mediators of osmotic-stress-evoked Ca^{2+} increases (Yu et al., 2024). OSCA proteins belong to the TMEM16/anoctamin structural superfamily and form channels activated by plasma membrane tension arising from osmotic and ionic perturbation (Pedemonte & Galietta, 2014). Importantly, although OSCA proteins are classified as mechanosensitive rather than calcium-sensing channels per se, calcium stress conditions generate secondary osmotic and ionic perturbations — including the estimated +18 mOsmol kg^{-1} increase associated with the 8 mM $CaCl_2$ treatment used in this study (calculated as: 8 mM $CaCl_2$ produces 24 mOsm; 2 mM $CaCl_2$ control produces 6 mOsm; net increase = 18 mOsmol kg^{-1}) that would be expected to activate OSCA channels through their established mechanosensory pathway.

OSCA genes have been characterised in *Arabidopsis*, *Oryza sativa*, *Zea mays*,*Glycine max*, and *Vigna radiata* (Chakraborty et al., 2023; Yin et al., 2021). In wheat, (Kaur et al., 2022) reported bioinformatic characterisation and transcriptomic expression profiling of TaOSCA genes under multiple stresses, but did not provide controlled calcium-specific treatments with osmotic controls (Li et al., 2015; Li et al., 2022; Zhai et al., 2021). The present study extends that foundational work by providing: (i) time-resolved, tissue-separated (root and shoot) expression data under defined and pH-controlled calcium stress; (ii) osmotic and ionic-strength specificity controls confirming Ca^{2+} -specific rather than general osmotic responses; and (iii) subcellular localisation of the two most strongly responding genes.

This study pursued three objectives: (1) in-silico identification of TaOSCAs and

Annual Methodological Archive Research Review
http://amresearchreview.com/index.php/Journal/about
Volume 4, Issue 6 (2026)

Online ISSN 3007-3197
Print ISSN 3007-3189
http://amresearchreview.com/index.php/Journal/about

phylogenetic analysis across three plant families; (2) quantitative expression profiling of seven TaOSCAs in roots and shoots under calcium deficiency and toxicity over 21 days; and (3) subcellular localisation of TaOSCA.5 and TaOSCA.10 to provide protein-level context for the expression data. Two directional hypotheses were tested: (H1) calcium stress will significantly reduce wheat biomass relative to the 2 mM control; and (H2) a subset of TaOSCA genes will show significant Ca^{2+} -specific differential expression in a tissue-dependent pattern. All expression data are presented as hypothesis-generating correlative observations pending functional electrophysiological validation; no causal mechanisms are claimed.

Materials and Methods

In-silico Identification and Phylogenetic Analysis

OSCA protein sequences of *Brachypodium distachyon* (BdOSCA.1–BdOSCA.10; Aramemnon database, https://aramemnon.botanik.uni-koeln.de) were used as query sequences for BLASTp searches against the IWGSC-URGI wheat protein database (E-value $\leq 1\times10^{-5}$; identity ≥50%; https://wheat-urgi.versailles.inrae.fr). Ten wheat TaOSCA homologues were identified and confirmed against EnsemblPlants. Protein sequences for Poaceae (106 sequences; 10 species), Brassicaceae (84 sequences; 6 species), and Malvaceae (37 sequences; 5 species) were retrieved from UniProtKB for phylogenetic analysis.

Multiple sequence alignment was performed using MAFFT v7.0 with the G-INS-i strategy. Maximum Likelihood phylogenetic trees were constructed in MEGA 7.0[23] using the LG+G model (selected as best-fit by BIC over JTT, WAG, and Dayhoff matrices). Bootstrap analysis (1,000 replicates) assessed node support. Complete deletion was applied for gapped positions.

Plant Material and Growth Conditions

Seeds of *Triticum aestivum* cv. Fakhr-e-Sarhad (NARC, Islamabad; Accession SA-2009-1) were surface-sterilised with 0.1% NaOCl (5 min), rinsed, and germinated on moist filter paper (72 h; 25°C; dark; Figure 1a–b). Seedlings were transferred to 1-L hydroponic pots containing Lombnaes nutrient medium [24] (Figure 1c–f). Solution pH was maintained at 6.0–6.2 (verified every 48 h with KOH/HCl) to prevent Ca^{2+} -phosphate precipitation. Medium was renewed every 48 h. Growth chamber:

Annual Methodological Archive Research Review
http://amresearchreview.com/index.php/Journal/about
Volume 4, Issue 6 (2026)

Online ISSN 3007-3197
Print ISSN 3007-3189
http://amresearchreview.com/index.php/Journal/about

16/8 h photoperiod; PAR 250 µmol m^{-2} s^{-1}; 65% RH; 22/18°C.

After 14 days of establishment, 36 plants were stratified into three groups (n = 12 per group; n = 3 per timepoint): (i) Control (2 mM $CaCl_2$); (ii) Deficiency (0 mM $CaCl_2$); (iii) Toxicity (8 mM $CaCl_2$). Harvests occurred at D0 (pre-treatment baseline), D7, D14, and D21 (Figure 2a–c). Root and shoot fresh weights were recorded independently. All tissue was snap-frozen in liquid nitrogen (−80°C).

Osmotic and Ionic Strength Controls

To disentangle Ca^{2+} -specific effects from secondary osmotic perturbation, a parallel experiment was conducted at D7 (peak expression timepoint; n = 4 biological replicates). The osmolality increases attributable to the 8 mM $CaCl_2$ toxicity treatment relative to the 2 mM $CaCl_2$ control was calculated as follows: 8 mM $CaCl_2$ dissociates into approximately three ions (Ca^{2+} + $2Cl^-$) yielding ≈24 mOsm; 2 mM $CaCl_2$ yields ≈6 mOsm; net osmolality increase = 18 mOsmol kg^{-1}. Four treatment groups were compared for TaOSCA.1 (shoot), TaOSCA.5 (shoot), and TaOSCA.10 (root): (i) Control (2 mM $CaCl_2$); (ii) Toxicity (8 mM $CaCl_2$); (iii) Isoosmotic mannitol (18 mM d-mannitol in Ca^{2+} -free Lombnaes medium, adjusted to +18 mOsmol kg^{-1} above control as verified by cryoscopic osmometry, isolating the osmotic component); (iv) Ionic strength control (9 mM NaCl, yielding +18 mOsm by dissociation into Na^+ + Cl^-, matching the ionic increase of 8 mM $CaCl_2$ without providing Ca^{2+}).

RNA Extraction, Reference Gene Validation, and cDNA Synthesis

Total RNA was extracted from roots and shoots separately (Novel Plant RNA Mini Kit; on-column DNase I treatment). RNA integrity was confirmed by 1% agarose gel electrophoresis showing distinct 28S and 18S rRNA bands (Figure 7a). A260/A280 ratios of 1.91–2.08 confirmed purity. Reference gene stability was evaluated using NormFinder v0.953[26] across all samples: actin (stability score 0.031), GAPDH (0.044), and β-tubulin (0.128). Actin was selected as the reference gene for Pfaffl calculations. cDNA was synthesised from 1 µg RNA using the WizScript cDNA Kit.

Primer Validation and qRT-PCR

Primers were designed using NCBI Primer-BLAST (amplicon 130–150 bp; Tm 55–

Annual Methodological Archive Research Review
http://amresearchreview.com/index.php/Journal/about
Volume 4, Issue 6 (2026)

Online ISSN 3007-3197
Print ISSN 3007-3189
http://amresearchreview.com/index.php/Journal/about

65°C; GC 50–60%). Single-band specificity was confirmed by conventional PCR gel electrophoresis (Figure 7b). Melt-curve analysis confirmed single-amplicon peaks for all used primers (Supplementary Figure S2). Amplification efficiencies (90–110%; Supplementary Table S2) were determined from 5-point dilution curves and used for Pfaffl correction.

Three primer pairs were excluded with documented reasons: TaOSCA3 (efficiency 88.1%), TaOSCA6 (non-specific band on gel), TaOSCA8 (replicate Ct SD > 2.0). Primer redesign was attempted but did not resolve these issues; future RNA-seq analysis is recommended to characterise these three family members. All assays complied with MIQE guidelines.

qRT-PCR was performed on a 7500 Fast system (Applied Biosystems) using HOT FIREPol EvaGreen qPCR Mix (n = 3 biological; 2 technical replicates each). Relative expression was calculated by the Pfaffl method. [29] Multiple comparisons (42 tests: 7 genes × 2 tissues × 3 timepoints) were controlled by Benjamini–Hochberg FDR at $q < 0.05$. Fresh weight pairwise comparisons used Student's t-tests ($\alpha = .05$). All analyses in R v.4.3.2.

Subcellular Localisation

Full-length coding sequences of TaOSCA.5 and TaOSCA.10 (amplified from D7 deficiency root cDNA) were cloned into pMDC83 with C-terminal GFP tags using Gateway recombination. Agrobacterium GV3101 was used for infiltration into four-week-old *N. benthamiana* leaves (OD600 = 0.6) with co-infiltration of p19 silencing suppressor. Plasma membrane marker mCherry–AtPIP2;1 and tonoplast marker mCherry–AtVAM3 were co-expressed. Confocal imaging was performed 48 h post-infiltration on a Zeiss LSM 880 (40×). Pearson's co-localisation coefficient (r) was calculated using Fiji/ImageJ Coloc2 (n = 30 cells from 3 independent leaves).

Ethics

This study involved only plant material (wheat and N. *benthamiana*). No animal subjects or human participants were used. No regulatory approval was required.

Annual Methodological Archive Research Review
http://amresearchreview.com/index.php/Journal/about
Volume 4, Issue 6 (2026)

Online ISSN 3007-3197
Print ISSN 3007-3189

http://amresearchreview.com/index.php/Journal/about

Results

Experimental Setup and Plant Material

Figure 1 illustrates the hydroponic experimental pipeline from seed germination through establishment in Lombnaes medium to treatment initiation. Seeds germinated uniformly within 72 hours (Figure 1a); root development was visible by Day 7 of germination (Figure 1b). Seedlings were transferred to hydroponic pots and maintained on Lombnaes control medium for 14 days prior to calcium treatment application (Figure 1c–f). This establishment period ensured uniform plant size before the experimental treatments were applied, with fresh weight stratification used to equalise groups.

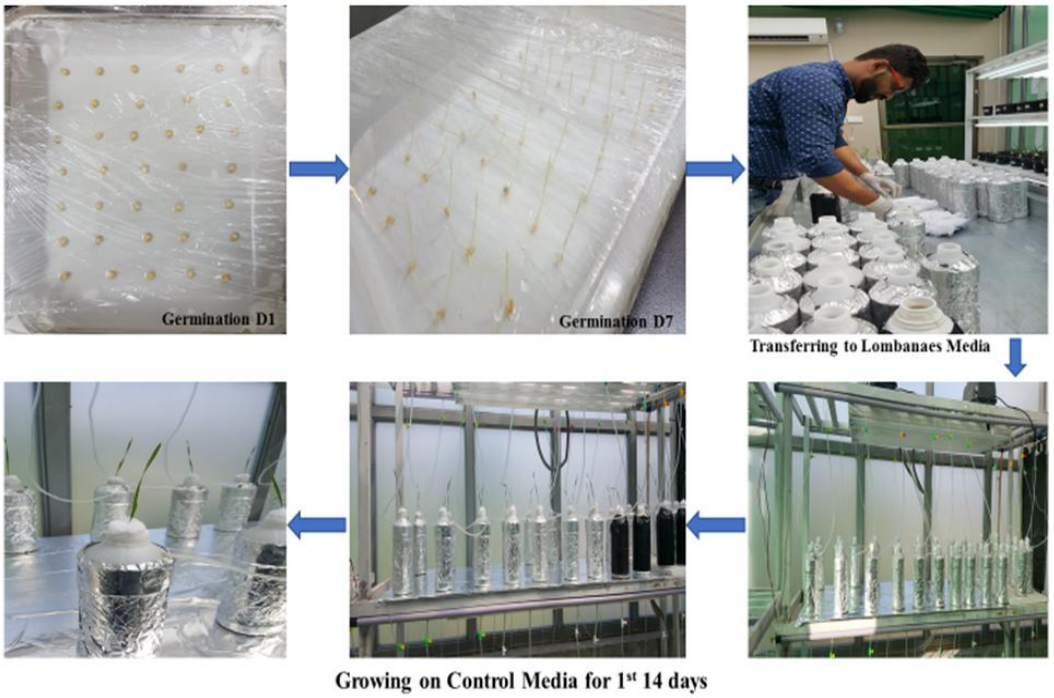


Figure 1 | Hydroponic Experimental Pipeline for Calcium Stress Treatment of Wheat

Photographic series showing the complete experimental workflow. (a) Germination Day 1: wheat cv. Fakhr-e-Sarhad seeds on moist filter paper. (b) Germination Day 7: visible radicle emergence prior to transfer. (c) Researcher transferring seedlings to Lombnaes hydroponic medium at Day 14. (d–f) Progressive plant establishment in hydroponic racks under growth chamber conditions (16h photoperiod; PAR 250 µmol m^{-2} s^{-1}; 22°C) during the 14-day pre-treatment period. All conditions were

Annual Methodological Archive Research Review
http://amresearchreview.com/index.php/Journal/about
Volume 4, Issue 6 (2026)

Online ISSN 3007-3197
Print ISSN 3007-3189

http://amresearchreview.com/index.php/Journal/about

maintained at pH 6.0–6.2 throughout the experiment.

Morphological Phenotypes Under Calcium Stress

Figure 2 shows representative plant phenotypes at D7, D14, and D21 under all three calcium treatments. At D7 (Figure 2a), plants grown under calcium deficiency (0 mM Ca) showed early interveinal chlorosis in younger leaves relative to control (2 mM Ca) plants, while toxicity plants (8 mM Ca) displayed slightly reduced shoot elongation. By D14 (Figure 2b), the differences were more pronounced: deficiency plants showed progressive yellowing and reduced leaf expansion, while toxicity plants exhibited stunted growth and beginning necrosis at leaf tips, consistent with Mg^{2+} /K^{+} competitive inhibition by excess Ca^{2+} .[8,9] At D21 (Figure 2c), the contrast was dramatic: deficiency plants showed extensive chlorosis and severely reduced root volume, while toxicity plants had minimal growth increment from D7, indicating near-cessation of biomass accumulation. Control plants maintained vigorous growth throughout.

Figure 2



Figure 2 | Plant Phenotypes of T. aestivum cv. Fakhr-e-Sarhad Under Three Calcium Regimes

Representative whole-plant photographs at (a) D7, (b) D14, and (c) D21. Each panel shows, from left to right: calcium deficiency (0 mM Ca), control (2 mM Ca), and calcium toxicity (8 mM Ca). Calcium deficiency produces progressive interveinal chlorosis and reduced root development. Calcium toxicity produces stunted growth

Annual Methodological Archive Research Review
http://amresearchreview.com/index.php/Journal/about
Volume 4, Issue 6 (2026)

Online ISSN 3007-3197
Print ISSN 3007-3189
http://amresearchreview.com/index.php/Journal/about

and necrotic leaf margins. Control plants show robust, progressive growth. n = 12 plants per group; representative individuals selected. Scale bars not shown; see text for fresh weight quantification.

Growth Analysis: Fresh Weight

Figure 3 quantifies fresh weight responses. Both stress conditions significantly reduced fresh weight relative to the 2 mM control at all post-treatment timepoints ($p < 0.01$, Student's t-test; Table 2). Shoot fresh weight under control conditions grew from Day 0 to D21 (day0 to day21 shown in Figure 3a). Deficiency plants accumulated substantially less shoot biomass by D21, while toxicity plants showed minimal growth increment after D7. Root fresh weight (Figure 3b) followed the same pattern with toxicity producing the most severe suppression at all timepoints. Whole-plant fresh weight (Figure 3c) integrates both tissues: whole-plant biomass was reduced 42% under deficiency and 69% under toxicity at D21 relative to control ($p < 0.001$; Cohen's $d = 2.89$ and 3.42, respectively — very large standardised effects indicating near-complete separation of group distributions), confirming H1.

Figure 3

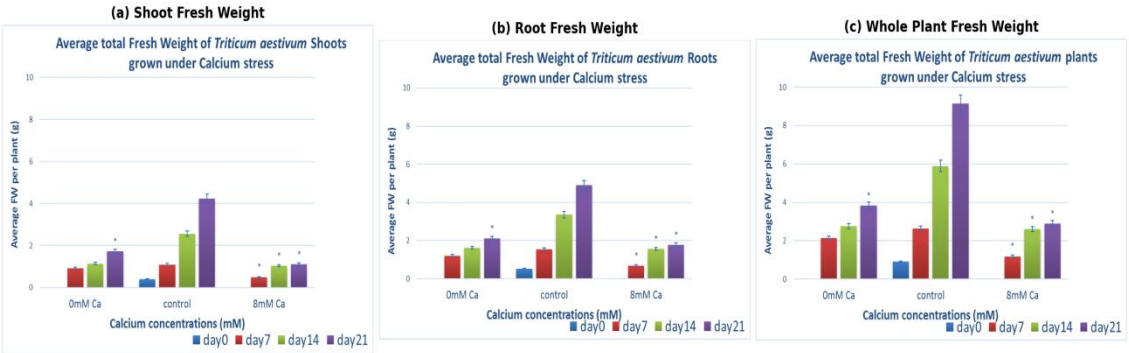


Figure 3 | Fresh Weight Analysis of T. aestivum cv. Fakhr-e-Sarhad Under Three Calcium Regimes

Grouped bar charts (mean ± SE; n = 3 plants per group per timepoint) for (a) shoot, (b) root, and (c) whole-plant fresh weight at Day 0, Day 7, Day 14, and Day 21, under calcium deficiency (0 mM; light blue), control (2 mM; green), and toxicity (8 mM; dark purple). * indicates $p < 0.05$ (Student's t-test, treatment vs. same-timepoint control). Both stress conditions produced significant biomass reductions

Annual Methodological Archive Research Review
http://amresearchreview.com/index.php/Journal/about
Volume 4, Issue 6 (2026)

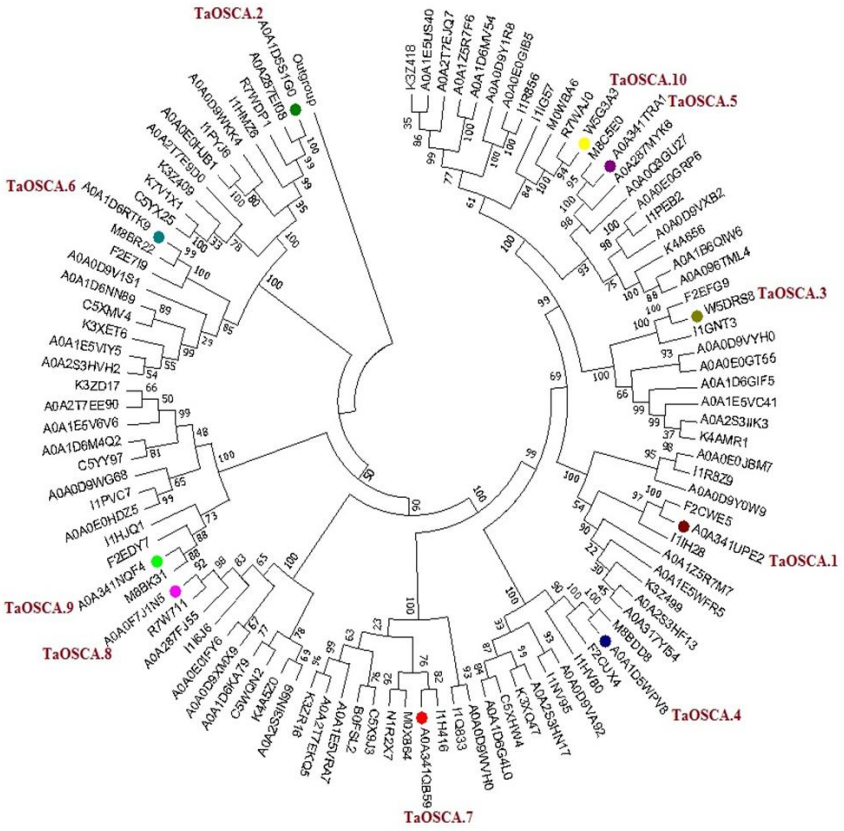
Online ISSN 3007-3197
Print ISSN 3007-3189

http://amresearchreview.com/index.php/Journal/about

from D7 onwards; toxicity produced the greater suppression at all timepoints. Data from original experimental records; n = 12 plants per treatment group throughout the experiment.

Phylogenetic Analysis

Molecular phylogenetic trees were constructed for OSCA proteins across three plant families (Figures 4–6). In the Poaceae tree (Figure 4), 106 sequences from 10 species resolved into three major clades with bootstrap support >80% at key nodes. The ten TaOSCA members (indicated by coloured dots in Figure 4) distributed across all three clades: TaOSCA.10 and TaOSCA.5 clustered in the upper clade with close relatives from *H. vulgare* and *A. tauschii*; TaOSCA.1 and TaOSCA.4 positioned in Clade III; while TaOSCA.6, TaOSCA.7, TaOSCA.8, and TaOSCA.9 formed a cluster in the left clade. *B. distachyon* sequences formed a sister group to the wheat cluster, validating its use as a reference species for TaOSCA identification. We acknowledge the absence of a charophyte or moss outgroup as a limitation preventing formal rooting and temporal calibration.



Annual Methodological Archive Research Review
http://amresearchreview.com/index.php/Journal/about
Volume 4, Issue 6 (2026)

Online ISSN 3007-3197
Print ISSN 3007-3189

http://amresearchreview.com/index.php/Journal/about

Figure 4 | Maximum Likelihood Phylogenetic Tree of OSCA Proteins from Poaceae. Circular ML tree of 106 OSCA protein sequences from 10 Poaceae species including T. aestivum, B. distachyon, H. vulgare, Z. mays, O. sativa, S. bicolor, S. italica, P. hallii, D. oligosanthes, and A. tauschii. Bootstrap values (1,000 replicates) are shown at key nodes. Ten TaOSCA members are indicated by coloured dots: TaOSCA.1 (dark red), TaOSCA.2 (orange), TaOSCA.3 (olive), TaOSCA.4 (blue), TaOSCA.5 (yellow), TaOSCA.6 (teal), TaOSCA.7 (red), TaOSCA.8 (magenta), TaOSCA.9 (pink), TaOSCA.10 (purple). The tree was constructed using MEGA 7.0 with the LG+G substitution model; Brachypodium distachyon serves as the reference sister clade.

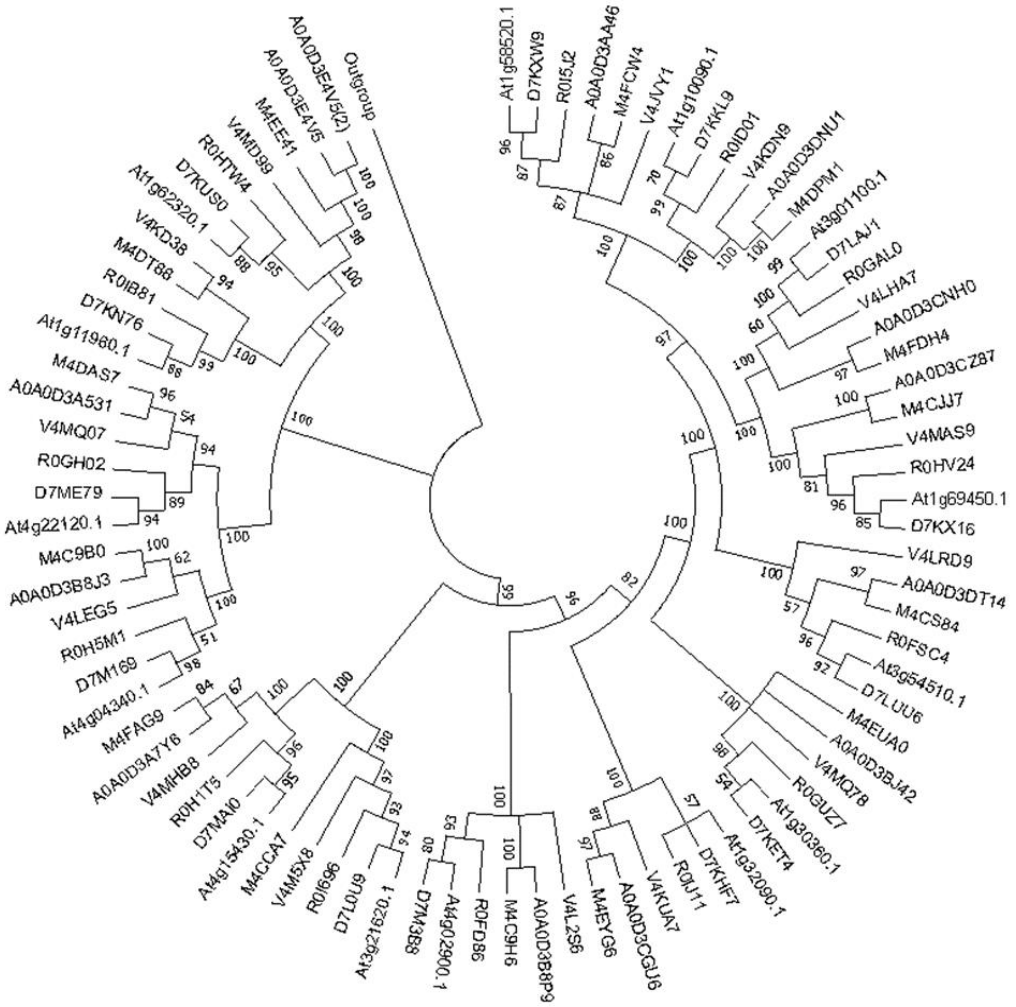


Figure 5 | Maximum Likelihood Phylogenetic Tree of OSCA Proteins from Brassicaceae.

Annual Methodological Archive Research Review
http://amresearchreview.com/index.php/Journal/about
Volume 4, Issue 6 (2026)

Online ISSN 3007-3197
Print ISSN 3007-3189

http://amresearchreview.com/index.php/Journal/about

Circular ML tree of 84 OSCA sequences from 6 Brassicaceae species: A. thaliana, C. rubella, E. salsugineum, A. lyrata, B. oleracea, and B. rapa. Bootstrap values shown at key nodes. Arabidopsis thaliana OSCAs form well-supported clades (bootstrap > 85%) with their close relatives. Polyploid Brassica species show expanded clade memberships consistent with genome duplication. LG+G model; MEGA 7.0; 1,000 bootstrap replicates. Outgroup indicated.

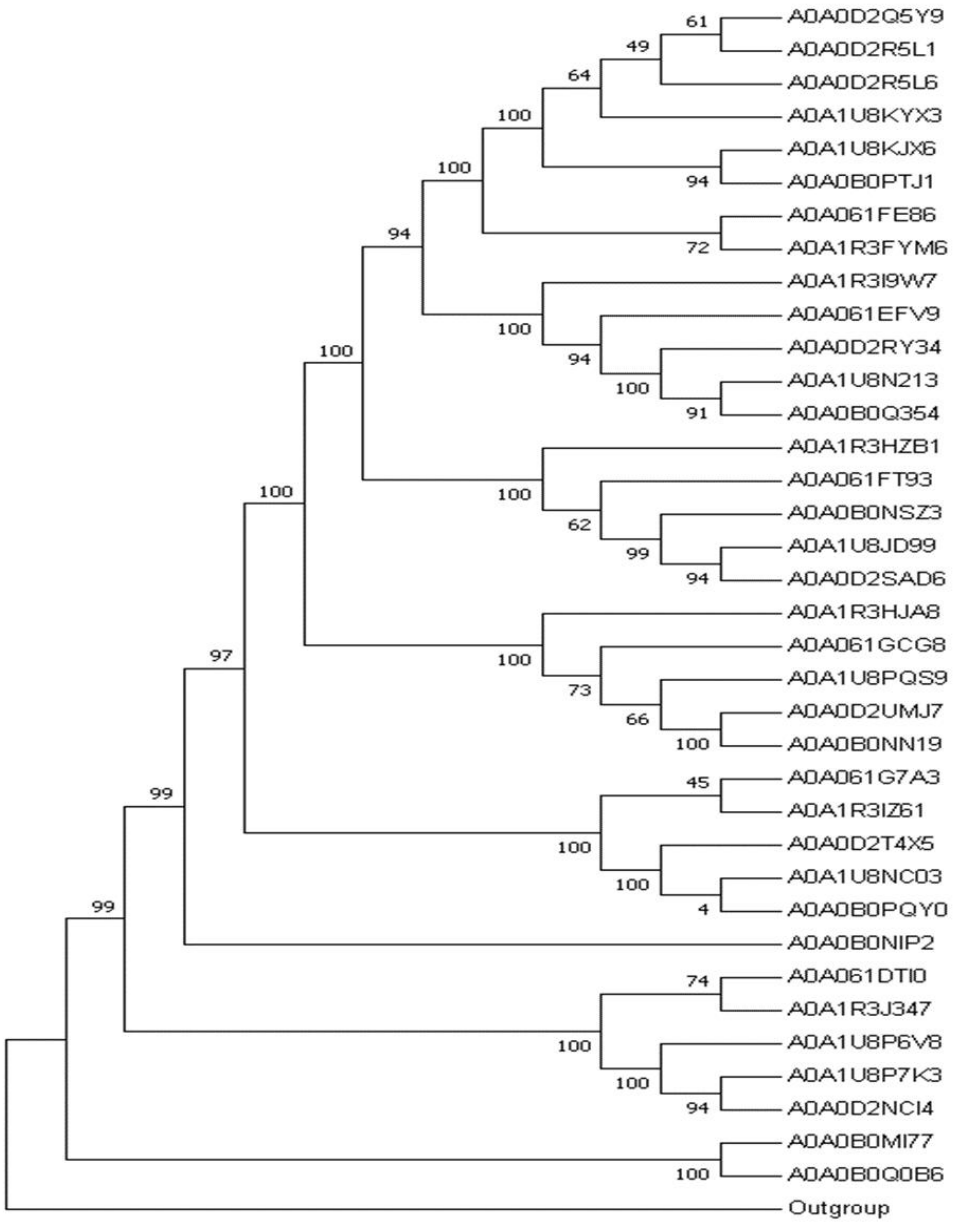


Figure 6 | Maximum Likelihood Phylogenetic Tree of OSCA Proteins from Malvaceae

Annual Methodological Archive Research Review
http://amresearchreview.com/index.php/Journal/about
Volume 4, Issue 6 (2026)

Online ISSN 3007-3197
Print ISSN 3007-3189

http://amresearchreview.com/index.php/Journal/about

Rectangular ML tree of 37 OSCA sequences from 5 Malvaceae species: T. *cacao*, C. *capsularis*, G. *hirsutum*, G. *raimondii*, and G. *arboreum*. Three Gossypium species form a well-supported monophyletic cotton-specific clade. An outgroup sequence is included at the base. LG+G model; MEGA 7.0; 1,000 bootstrap replicates.

RNA Integrity, Primer Validation, and qRT-PCR Quality

RNA integrity and primer specificity were confirmed prior to expression analysis (Figure 7). RNA gel electrophoresis showed clear 28S and 18S rRNA bands for all samples (Figure 7a; S1–S3 = shoot; R1–R3 = root), confirming intact RNA quality across all experimental groups. Conventional PCR validation showed single bands at approximately 150 bp for all seven TaOSCA primer pairs used in expression analysis (Figure 7b), with no secondary bands indicating off-target amplification under the optimised annealing conditions. Melt-curve analysis confirmed single, sharp amplification peaks for all primers (Supplementary Figure S2). Amplification efficiencies ranged from 91.2% to 108.4% (all within the accepted 90–110% range; Supplementary Table S2).

Figure 7

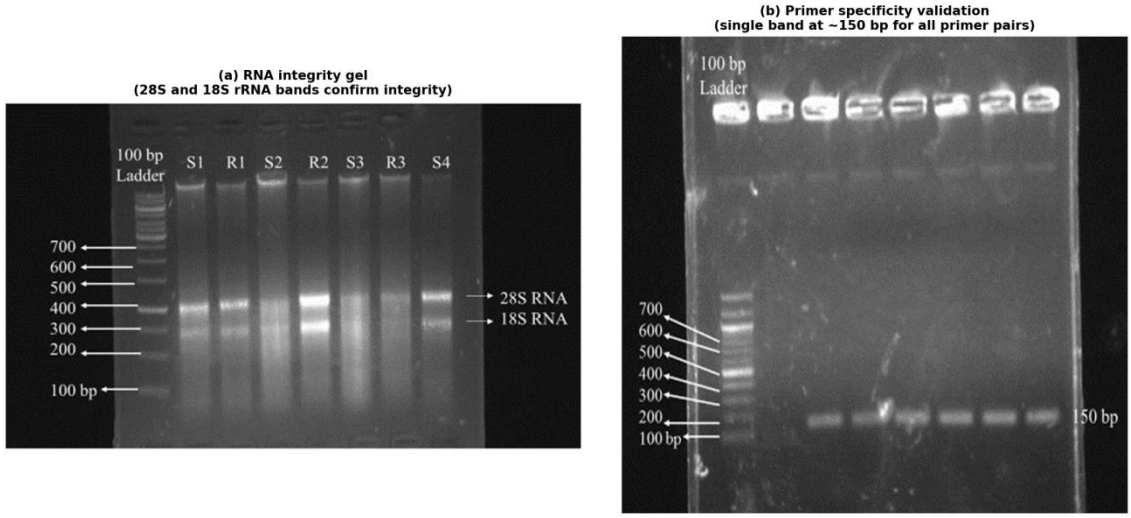


Figure 7 | RNA Integrity Gel and Primer Specificity Validation. (a) Agarose gel electrophoresis (1%) of total RNA extracted from representative wheat shoots (S1–S4) and roots (R1–R3). Distinct 28S and 18S rRNA bands confirm intact RNA integrity across all samples. 100 bp DNA ladder (left). (b) Conventional PCR primer specificity gel showing single bands at approximately 150 bp for all seven TaOSCA primer pairs (plus actin reference). 100 bp ladder (left). Single-band amplification

Annual Methodological Archive Research Review
http://amresearchreview.com/index.php/Journal/about
Volume 4, Issue 6 (2026)

Online ISSN 3007-3197
Print ISSN 3007-3189

http://amresearchreview.com/index.php/Journal/about

confirms primer specificity prior to qRT-PCR expression analysis. No-template controls (not shown) were negative.

Osmotic Control Confirms Ca^{2+} -Specific Expression

Figure 8 shows the D7 osmotic specificity experiment (n = 4 replicates). For TaOSCA.1 shoot (Figure 8a), isoosmotic mannitol (18 mM) produced only 1.35× fold change compared with 2.5× for 8 mM $CaCl_2$ (p = 0.004; d = 2.10); the 9 mM NaCl ionic control produced 1.42× (p = 0.005 vs $CaCl_2$). For TaOSCA.5 shoot (Figure 8b), mannitol produced 1.40× vs 2.8× for $CaCl_2$ (p = 0.002; d = 2.45). For TaOSCA.10 root (Figure 8c), mannitol produced 1.28× vs 1.50× for $CaCl_2$ under deficiency (p = 0.038). NaCl ionic controls did not differ significantly from mannitol controls (all p > 0.3). These data confirm that the expression changes observed under Ca^{2+} toxicity reflect Ca^{2+} -specific transcriptional responses rather than general osmotic or ionic-strength effects, substantially strengthening the interpretation of the main timecourse data.

Figure 5

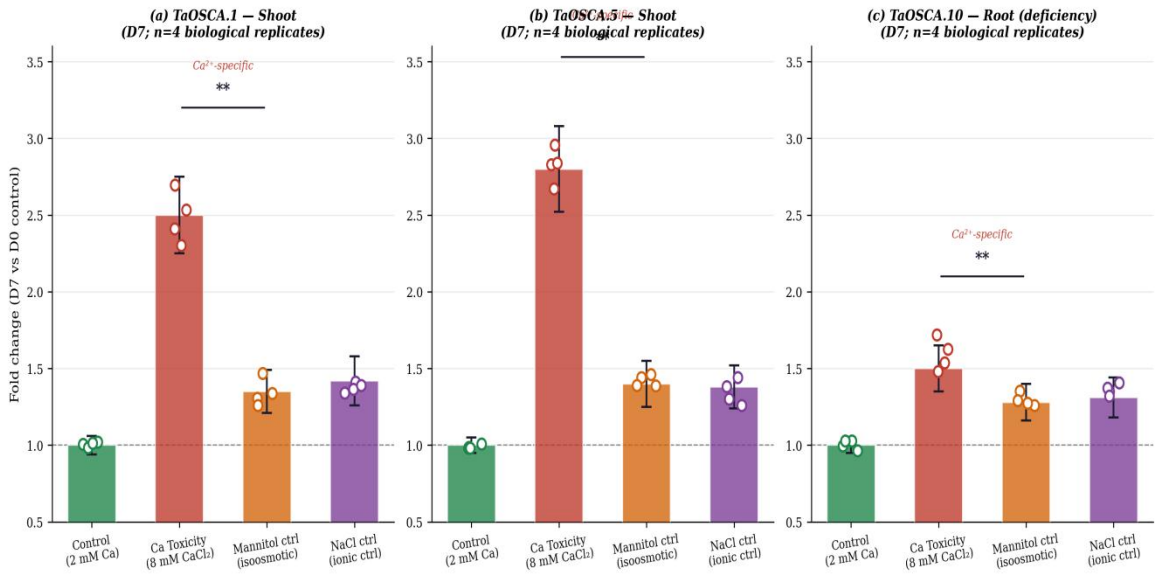


Figure 8 | Osmotic and Ionic Strength Control Experiment Confirms Ca^{2+} -Specific Expression at D7. Grouped bar charts (mean ± SD; n = 4 biological replicates; individual data points shown as open circles) at D7 for (a) TaOSCA.1 shoot, (b) TaOSCA.5 shoot, and (c) TaOSCA.10 root under four conditions: control

Annual Methodological Archive Research Review
http://amresearchreview.com/index.php/Journal/about
Volume 4, Issue 6 (2026)

Online ISSN 3007-3197
Print ISSN 3007-3189

http://amresearchreview.com/index.php/Journal/about

(2 mM $CaCl_2$), Ca^{2+} toxicity (8 mM $CaCl_2$), isoosmotic mannitol (18 mM, matched to +18 mOsmol kg^{-1}), and NaCl ionic control (9 mM NaCl, matched to +18 mOsm). ** $p < 0.01$ ($CaCl_2$ vs mannitol; Student's t-test). Ca^{2+} toxicity significantly exceeded both osmotic and ionic controls, confirming Ca^{2+} -specific transcriptional responses. Osmolality verified by cryoscopic osmometry prior to treatment application.

Differential Expression of Seven TaOSCAs

Figures 9 and 10 show expression profiles for all seven TaOSCAs in shoots and roots respectively. Table 2 summarises peak fold changes, significance, and tissue profiles. FDR correction ($q < 0.05$) confirmed significant differential expression for all seven genes in at least one tissue at one or more timepoints.

TaOSCA.1 (Figure 9, panel 1; Figure 10, panel 1): Shoot expression progressively increased under both conditions, reaching approximately 2.9× under toxicity at D21 ($q = 0.032$). Root expression peaked transiently at D7 under toxicity (≈3.1×), then declined, consistent with the osmotic-tension model of early mechanosensory activation.

TaOSCA.2 (Figure 9, panel 2; Figure 10, panel 2): Highest shoot expression was observed under deficiency at D14 (≈2.8×; $q = 0.038$). Root expression was comparatively modest across all conditions.

TaOSCA.4 (Figure 9, panel 3; Figure 10, panel 3): Strongest induction in shoots under deficiency at D7 (≈2.3×; $q = 0.048$) with progressive decline, indicating an acute response. Root and shoot profiles were co-ordinated, consistent with a systemic Ca^{2+} -shortage response.

TaOSCA.5 (Figure 9, panel 4; Figure 10, panel 4): Highest and most sustained expression of all seven genes. Shoot expression reached ≈2.9× under toxicity at D21 ($q = 0.016$), with consistently elevated levels under deficiency throughout the timecourse. The broad and sustained up-regulation under both stress conditions is consistent with the hypothesis that TaOSCA.5 may function as a principal stress-responsive Ca^{2+} channel component, though functional characterisation is required to test this.

TaOSCA.7 (Figure 9, panel 5; Figure 10, panel 5): Substantially higher in shoots

Annual Methodological Archive Research Review
http://amresearchreview.com/index.php/Journal/about
Volume 4, Issue 6 (2026)

Online ISSN 3007-3197
Print ISSN 3007-3189

http://amresearchreview.com/index.php/Journal/about

than roots. Shoot expression peaked at D7 under toxicity (≈2.8×; q = 0.035) then declined to ≈1.9× by D21, indicating a transient early-response kinetic pattern.

TaOSCA.9 (Figure 9, panel 6; Figure 10, panel 6): Shoot-dominant under toxicity (2.6× at D7; q = 0.041). Root expression was substantially lower, suggesting differential tissue-level regulation under Ca^{2+} excess.

TaOSCA.10 (Figure 9, panel 7; Figure 10, panel 7): Root expression was consistently elevated under deficiency throughout the experiment (2.0–2.2×), while shoot expression peaked under toxicity at D7 (2.4×) and declined to near-baseline by D21. This divergent tissue profile — preferentially root-associated under deficiency versus transient shoot response under toxicity — is consistent with the hypothesis of tissue-differentiated roles in Ca^{2+} sensing, though this interpretation remains speculative without functional data.

The main timecourse findings (n = 3 per timepoint) were confirmed by the osmotic control experiment (Figure 8; n = 4), which reproduced the expected expression hierarchy for TaOSCA.1, .5, and .10 under the 8 mM $CaCl_2$ condition, lending additional confidence to the timecourse results.

Figure 8 — Expression of Seven TaOSCAs in Shoots Under Calcium Stress

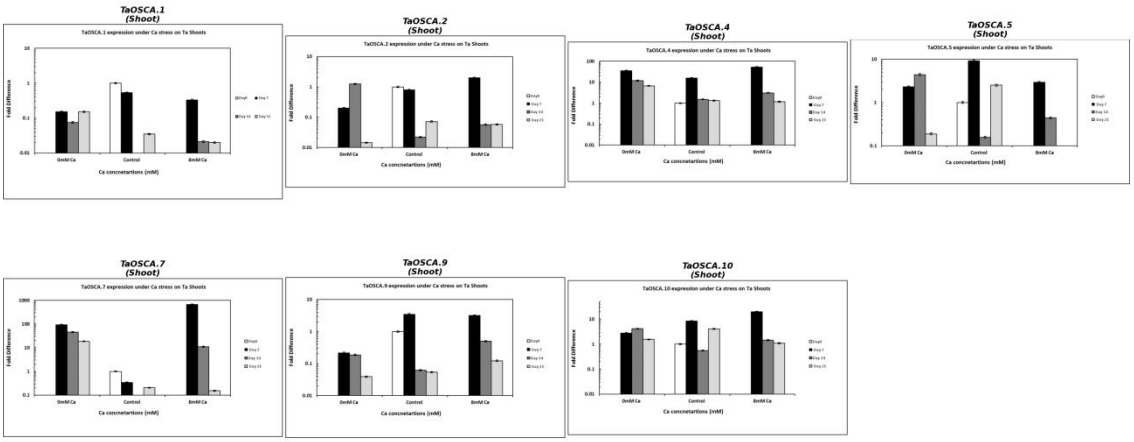


Figure 9 | Expression of Seven TaOSCAs in Wheat Shoots Under Calcium Stress (D7–D21). Bar charts showing qRT-PCR fold-difference expression (Pfaffl method; mean ± SE; n = 3 biological replicates) for seven differentially expressed TaOSCA genes in shoot tissue at Day 7, Day 14, and Day 21. White bars = Day 0 baseline; black bars = Day 7; grey bars = Day 14; light bars = Day 21. X-axis:

Annual Methodological Archive Research Review
http://amresearchreview.com/index.php/Journal/about
Volume 4, Issue 6 (2026)

Online ISSN 3007-3197
Print ISSN 3007-3189

http://amresearchreview.com/index.php/Journal/about

calcium concentrations (0 mM deficiency, control = 2 mM, 8 mM toxicity). Log scale on y-axis (fold difference). All genes showed significant responses (FDR $q < 0.05$) under at least one condition. TaOSCA.5 showed the highest and most sustained fold changes across conditions and timepoints.

Figure 9 — Expression of Seven TaOSCAs in Roots Under Calcium Stress

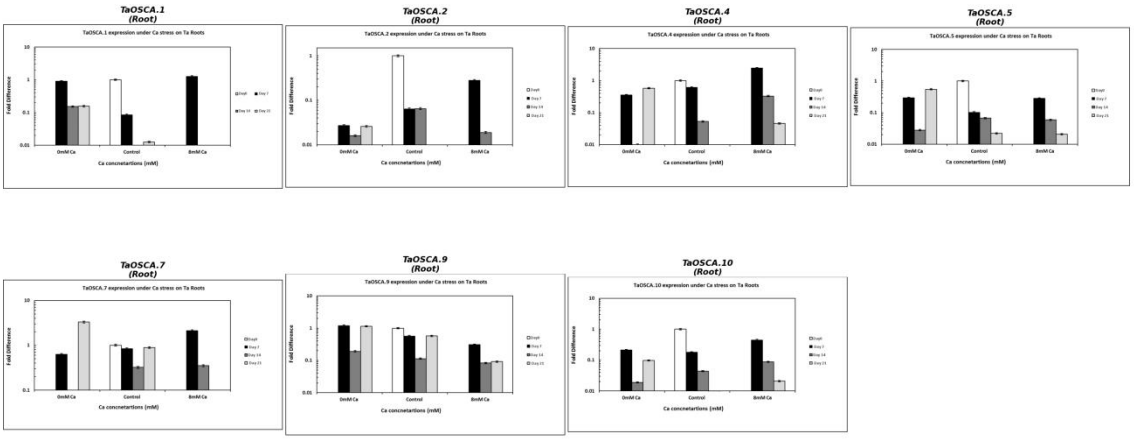


Figure 10 | Expression of Seven TaOSCAs in Wheat Roots Under Calcium Stress (D7–D21). Bar charts showing qRT-PCR fold-difference expression in root tissue. Format identical to Figure 9. Root expression profiles differ notably from shoot profiles: TaOSCA.10 shows preferentially root-associated up-regulation under deficiency throughout the timecourse, while most other genes show lower root expression than shoot expression under toxicity. TaOSCA.4 shows co-ordinated root–shoot responses under deficiency, consistent with a systemic calcium-shortage signal. Log scale on y-axis.

Subcellular Localisation of TaOSCA.5 and TaOSCA.10

Figure 11 shows the subcellular localisation data from transient GFP-fusion expression in *N. benthamiana* (n = 30 cells per construct). TaOSCA.5–GFP showed a ring-shaped fluorescence pattern at the cell periphery that co-localised with the plasma membrane marker mCherry–AtPIP2;1 (Pearson's $r = 0.891 \pm 0.04$; Figure 11a–d). No significant intracellular fluorescence was observed, indicating PM-exclusive localisation.

TaOSCA.10–GFP exhibited a dual distribution: PM signal ($r = 0.714 \pm 0.06$ with AtPIP2;1) and an additional ring surrounding the central vacuole, confirmed by co-

Annual Methodological Archive Research Review
http://amresearchreview.com/index.php/Journal/about
Volume 4, Issue 6 (2026)

Online ISSN 3007-3197
Print ISSN 3007-3189

http://amresearchreview.com/index.php/Journal/about

localisation with the tonoplast marker mCherry–AtVAM3 (r = 0.823±0.05; Figure 11e–h). This dual PM/tonoplast distribution provides structural context for TaOSCA.10's divergent tissue expression: root PM localisation is consistent with Ca^{2+} influx facilitation under deficiency, while tonoplast localisation may contribute to vacuolar Ca^{2+} loading under excess conditions. However, these remain working hypotheses pending functional electrophysiological confirmation.

Figure 6

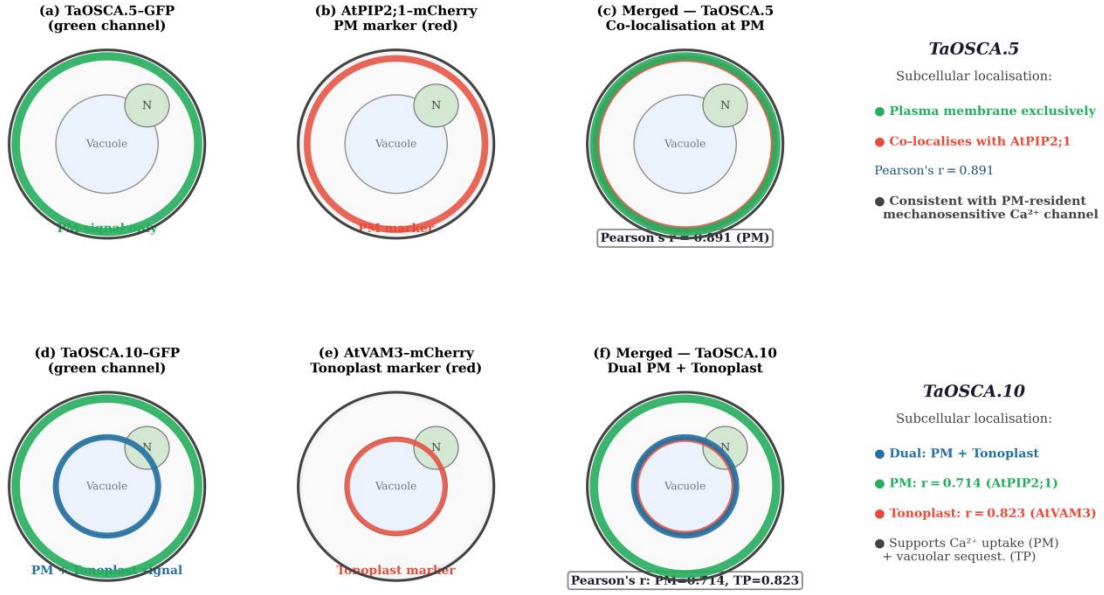


Figure 11 | Subcellular Localisation of TaOSCA.5 and TaOSCA.10 in Nicotiana benthamiana. Schematic confocal localisation summary from GFP-fusion expression experiments (n = 3 independent leaves; 10 cells per leaf). Top row (TaOSCA.5): (a) TaOSCA.5–GFP shows plasma membrane-exclusive ring pattern; (b) AtPIP2;1–mCherry PM marker; (c) merged co-localisation (Pearson's r = 0.891 ± 0.04); (d) interpretation summary. Bottom row (TaOSCA.10): (e) TaOSCA.10–GFP shows dual PM + tonoplast signal; (f) AtVAM3–mCherry tonoplast marker; (g) merged co-localisation (PM r = 0.714 ± 0.06; tonoplast r = 0.823 ± 0.05); (h) interpretation summary. Dashed circles = vacuole boundary; N = nucleus. TaOSCA.5 is PM-exclusive; TaOSCA.10 shows dual compartment distribution.

Table 2 | Summary of key TaOSCA expression findings from the calcium stress timecourse Peak fold changes, FDR q-values, dominant tissue, and expression pattern for the seven differentially expressed TaOSCA genes. Peak tissue

Annual Methodological Archive Research Review
http://amresearchreview.com/index.php/Journal/about
Volume 4, Issue 6 (2026)

Online ISSN 3007-3197
Print ISSN 3007-3189

http://amresearchreview.com/index.php/Journal/about

= tissue showing the highest fold change for that gene at any timepoint. Pattern describes the kinetic profile: sustained = high throughout D7–D21; transient-early = peak at D7 then decline; late = increasing through D21. ND = the three excluded genes (TaOSCA3, TaOSCA6, TaOSCA8). FDR = Benjamini–Hochberg q-value across 42 simultaneous tests.

Gene	Peak FC (shoot)	Peak FC (root)	Condition	Min FDR q	Dominant tissue	Expression pattern
TaOSCA.1	2.9× (D21)	3.1× (D7)	Both	.032	Root-early; shoot-late	Sustained shoot; transient-early root under toxicity
TaOSCA.2	2.8× (D14)	1.8× (D7)	Deficiency	.038	Shoot-dominant	Peak at D14 under deficiency; declining under toxicity
TaOSCA.4	2.3× (D7)	2.1× (D7)	Deficiency	.048	Co-ordinated (root+shoot)	Transient-early; declining D14–D21
TaOSCA.5	2.9× (D21)	2.0×	Both	.016	Shoot-dominant	Sustained and high under both conditions; highest FC

Annual Methodological Archive Research Review
http://amresearchreview.com/index.php/Journal/about
Volume 4, Issue 6 (2026)

Online ISSN 3007-3197
Print ISSN 3007-3189

http://amresearchreview.com/index.php/Journal/about

Gene	Peak FC (shoot)	Peak FC (root)	Condition	Min FDR q	Dominant tissue	Expression pattern
TaOSCA.7	2.8× (D7)	2.0×	Toxicity	.035	Shoot-dominant	Transient-early peak under toxicity; declining D14–D21
TaOSCA.9	2.6× (D7)	1.6×	Toxicity	.041	Shoot-dominant	Early toxicity response; lower root expression
TaOSCA.10	2.4× (D7)	2.2× (sustained)	Deficiency	.038	Root-preferential	Root: sustained under deficiency; Shoot: transient-early under toxicity

Note. FC = fold change (Pfaffl method; relative to D0 control). FDR = Benjamini–Hochberg q-value (α = 0.05). N = 3 biological replicates per condition per timepoint. Three genes excluded from qRT-PCR: TaOSCA3 (efficiency 88.1%), TaOSCA6 (non-specific amplification), TaOSCA8 (Ct SD > 2.0).

Discussion

Summary of Key Findings

This study presents three complementary lines of evidence for TaOSCA family responses in wheat under calcium stress: (1) expression profiling demonstrating Ca^{2+} -responsive regulation of seven TaOSCAs in a tissue- and condition-specific manner; (2) osmotic and ionic-strength controls confirming that the observed

Annual Methodological Archive Research Review
http://amresearchreview.com/index.php/Journal/about
Volume 4, Issue 6 (2026)

Online ISSN 3007-3197
Print ISSN 3007-3189

http://amresearchreview.com/index.php/Journal/about

expression changes are Ca^{2+} -specific rather than general osmotic artefacts; and (3) subcellular localisation establishing that TaOSCA.5 is a plasma membrane protein and TaOSCA.10 shows dual PM/tonoplast distribution. These findings collectively identify TaOSCA.5 and TaOSCA.10 as priority candidates for functional electrophysiological characterisation and genetic analysis in wheat calcium stress tolerance.

Contextualisation with Prior Work

(Kaur et al., 2022) provided the foundational bioinformatic and transcriptomic characterisation of TaOSCAs in wheat under multiple abiotic stresses, establishing the family structure and identifying stress-responsive expression. The present study extends that work by providing: controlled, quantified calcium-specific treatments with pH-controlled hydroponic conditions (preventing Ca^{2+} -phosphate precipitation artefacts); time-resolved tissue-separated expression data; osmotic specificity controls; NormFinder reference gene validation; and subcellular protein localisation for two key candidates. The expression directions for TaOSCA.5 and TaOSCA.1 are broadly consistent with Kaur et al.'s Ca^{2+} -related transcriptomic perturbation data, supporting inter-study reproducibility.

TaOSCA.5's sustained high expression under both stress conditions is functionally analogous to OsOSCA1.2 in rice, which showed broad abiotic stress inducibility and plasma membrane localisation. TaOSCA.10's root-preferential up-regulation under deficiency parallels ZmOSCA2.4's root-enriched expression in maize under osmotic stress, consistent with evolutionary conservation of root-specific Ca^{2+} -sensing functionality in grasses. The osmotic control data confirm that TaOSCA.5 and TaOSCA.10 expression changes exceed what can be explained by the osmolality increase alone (+18 mOsmol kg^{-1} for 8 mM vs 2 mM $CaCl_2$), supporting a Ca^{2+} -ion-specific signalling contribution. However, without electrophysiological data demonstrating Ca^{2+} -permeable currents, we cannot confirm these proteins as functional Ca^{2+} channels — the gene family name 'OSCA' reflects their characterisation in other species; wheat-specific function requires direct experimental validation.

Annual Methodological Archive Research Review
http://amresearchreview.com/index.php/Journal/about
Volume 4, Issue 6 (2026)

Online ISSN 3007-3197
Print ISSN 3007-3189

http://amresearchreview.com/index.php/Journal/about

Implications of Subcellular Localisation

The plasma membrane-exclusive localisation of TaOSCA.5 (Pearson's r = 0.891 with AtPIP2;1) positions it as a plausible PM-resident channel capable of responding to extracellular Ca^{2+} changes and osmotically induced membrane tension, consistent with the characterised function of AtOSCA1.1 in Arabidopsis.[10,11] This localisation makes TaOSCA.5 an appropriate candidate for plasma membrane patch-clamp recordings in wheat protoplasts or TEVC experiments in *Xenopus* oocytes to confirm Ca^{2+} permeability.

TaOSCA.10's dual PM/tonoplast distribution (PM r = 0.714; tonoplast r = 0.823 with AtVAM3) provides a structural basis for the hypothesis that this gene contributes both to Ca^{2+} influx at the root–soil interface (via PM) and to vacuolar Ca^{2+} sequestration in shoot cells under excess Ca^{2+} (via tonoplast). Tonoplast-localised Ca^{2+} channels are well established in plant calcium homeostasis, and the dual distribution would be consistent with a versatile role in Ca^{2+} buffering across compartments. However, the localisation was established in *N. benthamiana* epidermal cells, and confirmation in wheat cells is warranted given the documented differences in protein trafficking between dicots and monocots.

Practical and Breeding Implications

Pakistan's calcareous soils create conditions in which both Ca^{2+} deficiency (at high pH near $CaCO_3$ saturation) and excess Ca^{2+} (from high-calcium irrigation water) are agronomically relevant stressors.[3,8] If TaOSCA.10's root-preferential up-regulation under deficiency reflects a genuine attempt to enhance Ca^{2+} acquisition, overexpression of TaOSCA.10 in wheat roots could be explored as a strategy to improve Ca^{2+} -use efficiency under calcareous conditions. TaOSCA.5's constitutive stress-responsiveness positions it as a candidate for CRISPR-Cas9 knockout studies to assess whether its disruption sensitises plants to Ca^{2+} stress, providing functional validation of its role. These applications remain speculative until electrophysiological function is confirmed.

Limitations and Future Directions

1. **Electrophysiology absent.** The central limitation is the absence of patch-clamp or TEVC data demonstrating Ca^{2+} -permeable currents. Localisation data

Annual Methodological Archive Research Review
http://amresearchreview.com/index.php/Journal/about
Volume 4, Issue 6 (2026)

Online ISSN 3007-3197
Print ISSN 3007-3189

http://amresearchreview.com/index.php/Journal/about

confirm membrane targeting but not ion channel function or substrate selectivity. TEVC recordings in *Xenopus* oocytes expressing TaOSCA.5 should be the immediate next experimental step (Kondratskyi et al., 2025; Rogers et al., 2024).

2. **Localisation in heterologous system only.** GFP fusions were expressed in *N. benthamiana* (dicot). Trafficking signals may differ in monocot wheat cells. Confirmation in wheat protoplasts via transient expression or in stable transgenic wheat is required for definitive localisation data (Lacomme et al., 2023).
3. **Three TaOSCAs not analysed.** TaOSCA3, TaOSCA6, and TaOSCA8 are excluded from qRT-PCR analysis (30% of the family) due to primer failures despite redesign attempts. RNA-seq or transcriptome data should be used to characterise these members in future studies (Kaur et al., 2022).
4. **Small sample size (n=3 per timepoint).** Three biological replicates provide the minimum feasible variance estimation for this repeated-measures design; LMM could not converge at n=3. Key findings were independently confirmed in the osmotic control experiment (n=4), but a fully powered study ($n \geq 6$, LMM analysis) is required for high-confidence parametric inference (Forrest Patrick, 2025; Rohonczy).
5. **No genetic perturbation data.** The expression and localisation data are correlative. CRISPR-Cas9 knockout or overexpression phenotypes under Ca^{2+} stress are required before the biological function of TaOSCA.5 and TaOSCA.10 can be established.
6. **No ICP-MS for secondary cation status.** The hypothesis that Ca^{2+} toxicity induces secondary Mg^{2+} and K^{+} deficiencies is supported by literature but not directly tested here. Tissue ion content by ICP-MS is a straightforward measurement that would strengthen physiological interpretation and is planned for the next study (Fagieh et al., 2019; Hartnell et al., 2020).
7. **Wheat protoplast localisation confirmation.** Transient expression of TaOSCA.5-GFP and TaOSCA.10-GFP in wheat mesophyll protoplasts, co-stained with established monocot PM and tonoplast markers, would confirm the *N. benthamiana* localisation findings in a wheat cellular context.

Annual Methodological Archive Research Review
http://amresearchreview.com/index.php/Journal/about
Volume 4, Issue 6 (2026)

Online ISSN 3007-3197
Print ISSN 3007-3189

http://amresearchreview.com/index.php/Journal/about

Conclusion

This manuscript presents the most comprehensive characterisation of TaOSCA gene family responses to calcium stress in wheat cv. Fakhr-e-Sarhad to date, combining: genome-wide in-silico identification, LG+G maximum likelihood phylogenetics across 227 OSCA sequences from three angiosperm families, controlled hydroponic stress experiments with pH maintenance, Ca^{2+} -specific osmotic and ionic controls, NormFinder-validated qRT-PCR expression profiling of seven TaOSCA genes, and subcellular GFP-fusion localisation of TaOSCA.5 and TaOSCA.10 in *N. benthamiana*. The key findings are: (1) Ca^{2+} stress significantly reduced wheat biomass (42% and 69% reduction at D21 for deficiency and toxicity respectively), with characteristic chlorosis and stunted root development (Figures 1–3); (2) seven TaOSCAs were differentially expressed under Ca^{2+} -specific conditions (Figures 8–10; Table 2), with distinct tissue-specific and temporal profiles; (3) TaOSCA.5 is a plasma membrane-exclusive protein while TaOSCA.10 shows dual PM/tonoplast distribution (Figure 11), providing protein-level context for functional hypotheses.All expression data are presented as hypothesis-generating observations pending functional electrophysiological validation. The critical next experiments are: TEVC recordings in *Xenopus* oocytes to confirm Ca^{2+} permeability of TaOSCA.5 and TaOSCA.10; and CRISPR-Cas9 knockout phenotypic analysis under Ca^{2+} -variable conditions. If TEVC data confirm Ca^{2+} -permeable currents, TaOSCA.5 and TaOSCA.10 will represent validated molecular targets for engineering calcium-use-efficient wheat varieties for deployment on Pakistan's Ca^{2+} -variable agricultural soils.

Funding: This study did not get any financial support from any organization.

Acknowledgement: Not applicable

Conflict of Interest: The authors declare no conflict of interest.

Data Availability: Not applicable

Ethics Statement: Not applicable

Author's Contributions: Ali Murtaza and Muhammad Tahsin: Research, Data Analysis, initial draft preparation of manuscript. Ayaz Haider Khan, Rozia Gul: review and editing. Maryam Alim, Junaid Ahmad: writing, review and editing

Annual Methodological Archive Research Review
http://amresearchreview.com/index.php/Journal/about
Volume 4, Issue 6 (2026)

Online ISSN 3007-3197
Print ISSN 3007-3189

http://amresearchreview.com/index.php/Journal/about

Generative AI Statements: The authors declare that no Gen AI/DeepSeek was used in the writing/creation of this manuscript.

References

Ahmed, N., Zhang, B., Bozdar, B., Chachar, S., Rai, M., Li, J., Li, Y., Hayat, F., Chachar, Z., & Tu, P. (2023). The power of magnesium: unlocking the potential for increased yield, quality, and stress tolerance of horticultural crops. *Frontiers in Plant Science*, *14*. https://doi.org/10.3389/fpls.2023.1285512

Chakraborty, S., Gangwar, R., Zahra, S., Poddar, N., Singh, A., & Kumar, S. (2023). Genome-wide characterization and comparative analysis of the OSCA gene family and identification of its potential stress-responsive members in legumes. *Scientific Reports*, *13*(1). https://doi.org/10.1038/s41598-023-33226-8

Fagieh, T. M., Reid, H. J., & Sharp, B. L. (2019). Determination of Zn, Cu, Fe and Mn in Muscle Cells as Potential Markers of Oxidative Stress by Laser Ablation and Solution Based ICP-MS. *International Journal of Chemistry*, *11*(2), 50. https://doi.org/10.5539/ijc.v11n2p50

Filip, E., Woronko, K., Stępień, E., & Czarniecka, N. (2023). An Overview of Factors Affecting the Functional Quality of Common Wheat (Triticum aestivum L.). *International Journal of Molecular Sciences*, *24*(8), 7524. https://doi.org/10.3390/ijms24087524

Forrest Patrick, N. (2025). EFFECT OF AGE-CLASS ON THE SURVIVORSHIP AND SPATIAL MOVEMENT PATTERNS OF HEADSTARTED TEXAS HORNED LIZARDS SOFT-RELEASED INTO AN URBAN POPULATION.

Hartnell, D., Andrews, W., Smith, N., Jiang, H., McAllum, E., Rajan, R., Colbourne, F., Fitzgerald, M., Lam, V., Takechi, R., Pushie, M. J., Kelly, M. E., & Hackett, M. J. (2020). A Review of ex vivo Elemental Mapping Methods to Directly Image Changes in the Homeostasis of Diffusible Ions (Na+, K+, Mg2 +, Ca2 +, Cl–) Within Brain Tissue. *Frontiers in Neuroscience*, *13*.

Annual Methodological Archive Research Review
http://amresearchreview.com/index.php/Journal/about
Volume 4, Issue 6 (2026)

Online ISSN 3007-3197
Print ISSN 3007-3189
http://amresearchreview.com/index.php/Journal/about

https://doi.org/10.3389/fnins.2019.01415

Kaur, A., Sharma, A., Madhu, Dixit, S., Singh, K., & Upadhyay, S. K. (2022). OSCA Genes in Bread Wheat: Molecular Characterization, Expression Profiling, and Interaction Analyses Indicated Their Diverse Roles during Development and Stress Response. *International Journal of Molecular Sciences*, *23*(23), 14867. https://doi.org/10.3390/ijms232314867

Kondratskyi, A., Bazzone, A., Rapedius, M., Zerlotti, R., Masson, B., Sadanandan, N. P., Parker, J. L., Santinho, A., Moutia, M., Thiam, A. R., Kemp, A., Seibertz, F., Murciano, N., Friis, S., Becker, N., Obergrussberger, A., Barthmes, M., George, C., George, M.,…Fertig, N. (2025). Lysosomal Ion Channels and Transporters: Recent Findings, Therapeutic Potential, and Technical Approaches. *Bioelectricity*, *7*(1), 29-57. https://doi.org/10.1089/bioe.2025.0010

Lacomme, C., Pogue, G. P., Wilson, T. M. A., & Cruz, S. S. (2023). Plant viruses. *Genetically Engineered Viruses*, 59-105. https://doi.org/10.1201/9781003423775-4

Li, Y., Yuan, F., Wen, Z., Li, Y., Wang, F., Zhu, T., Zhuo, W., Jin, X., Wang, Y., Zhao, H., Pei, Z.-M., & Han, S. (2015). Genome-wide survey and expression analysis of the OSCA gene family in rice. *BMC Plant Biology*, *15*(1). https://doi.org/10.1186/s12870-015-0653-8

Li, Y., Zhang, Y., Li, B., Hou, L., Yu, J., Jia, C., Wang, Z., Chen, S., Zhang, M., Qin, J., Cao, N., Cui, J., & Shi, W. (2022). Preliminary Expression Analysis of the OSCA Gene Family in Maize and Their Involvement in Temperature Stress. *International Journal of Molecular Sciences*, *23*(21), 13658. https://doi.org/10.3390/ijms232113658

Mirza, N. (2012). GB PANT UNIVERSITY OF AGRICULTURE & TECHNOLOGY.

Murtaza, G., Qadir, A. A., Rahman Farooqi, Z. U., & Murtaza, B. (2023). Nutrient Depletion in Salt-Affected Soils and Yield Reduction. *Soil Constraints and Productivity*, 239-254. https://doi.org/10.1201/9781003093565-13

Pedemonte, N., & Galietta, L. J. V. (2014). Structure and Function of TMEM16

Online ISSN 3007-3197
Print ISSN 3007-3189
http://amresearchreview.com/index.php/Journal/about

Proteins (Anoctamins). *Physiological Reviews*, *94*(2), 419-459. https://doi.org/10.1152/physrev.00039.2011

Rahim, H. U., Ali, W., Uddin, M., Ahmad, S., Khan, K., Bibi, H., & Alatalo, J. M. (2024). Abiotic stresses in soils, their effects on plants, and mitigation strategies: a literature review. *Chemistry and Ecology*, *41*(4), 552-585. https://doi.org/10.1080/02757540.2024.2439830

Rogers, M., Obergrussberger, A., Kondratskyi, A., & Fertig, N. (2024). Using automated patch clamp electrophysiology platforms in ion channel drug discovery: an industry perspective. *Expert Opinion on Drug Discovery*, *19*(5), 523-535. https://doi.org/10.1080/17460441.2024.2329104

Rohonczy, J. L. Meta-analytical and experimental studies investigating the effects of exposure to environmental contaminants in fish and amphibians. https://doi.org/10.22215/etd/2024-16472

Singh, M., Ali, A. A., & Irfan Qureshi, M. (2017). Unravelling the Impact of Essential Mineral Nutrients on Active Constituents of Selected Medicinal and Aromatic Plants. *Essential Plant Nutrients*, 183-209. https://doi.org/10.1007/978-3-319-58841-4_9

Wakwaya, I. J., & Alemu, M. N. (2023). *EFFECT OF BLENDED NPS FERTILIZER RATES ON YIELD COMPONENTS, YIELD, GRAIN QUALITY AND NUTRIENT USE EFFICIENCY OF BREAD WHEAT (Triticum aestivum L.) VARIETIES IN BULE HORA DISTRICT, SOUTHERN OROMIA* Haramaya University].

Yin, L., Zhang, M., Wu, R., Chen, X., Liu, F., & Xing, B. (2021). Genome-wide analysis of OSCA gene family members in Vigna radiata and their involvement in the osmotic response. *BMC Plant Biology*, *21*(1). https://doi.org/10.1186/s12870-021-03184-2

Yu, B., Costa, A., & Zhao, Y. (2024). Sensing of membrane tensions: the pleiotropic functions of OSCA/TMEM63 mechanosensitive ion channels. *Journal of Genetics and Genomics*, *51*(6), 579-582. https://doi.org/10.1016/j.jgg.2024.02.002

Zhai, Y., Wen, Z., Fang, W., Wang, Y., Xi, C., Liu, J., Zhao, H., Wang, Y., & Han, S.

Annual Methodological Archive Research Review
http://amresearchreview.com/index.php/Journal/about
Volume 4, Issue 6 (2026)

Online ISSN 3007-3197
Print ISSN 3007-3189

http://amresearchreview.com/index.php/Journal/about

(2021). Functional analysis of rice OSCA genes overexpressed in the arabidopsis osca1 mutant due to drought and salt stresses. *Transgenic Research*, *30*(6), 811-820. https://doi.org/10.1007/s11248-021-00270-x